16th World Conference on Earthquake, 16WCEE 2017

Santiago Chile, January 9th to 13th 2017

Paper N° 1258 (Abstract ID)

Registration Code: S-V1462979610

Study of the liquefaction history in a lowland area in Tokyo caused by three earthquakes, including the Great East Japan Earthquake

S. Yasuda[(1)], K. Ishikawa[(2)], A. Takeda[(3)]

[(1)] *Professor, Dept. of Civil and Environmental Engineering, Tokyo Denki University, Japan, yasuda@g.dendai.ac.jp*
[(2)] *Assistant Professor, Dept. of Civil and Environmental Engineering, Tokyo Denki University, Japan, ishikawa@g.dendai.ac.jp*
[(3)] *Graduate Student, Tokyo Denki University, Japan, 15rmg09@ms.dendai.ac.jp*

Abstract

On March 11, 2011, the Great East Japan Earthquake occurred, causing extensive soil liquefaction over a wide range of land in Japan, resulting in extensive damage to wooden houses, water supplies, and sewer systems. The damage caused by liquefaction also occurred in the bay coast of landfills in Tokyo, though liquefaction did not occur in the alluvial lowland area in the immediate vicinity of Tokyo Bay. In these alluvial lowlands, the district along the old Sumida River has been previously affected by liquefaction caused by earthquakes, including the Great Kanto Earthquake, 1923 and the Edo Earthquake, 1855. The reasons why the area was affected by liquefaction during the past earthquakes, but was not affected during the Great East Japan Earthquake can be considered by the following two factors:

i) The ground had become unlikely to undergo liquefaction due to an “aging” effect, whereby the liquefaction strength of the soil gradually increased since the Great Kanto Earthquake occurred.

ii) The area had not undergone liquefaction, because the ground motion of the Great East Japan Earthquake was weaker than the past two earthquakes.

The tests were performed on the compacted specimen from one hour to a maximum of 100 days. Based on the results, the liquefaction strengths of the specimens that consolidated over longer periods of time were larger compared with specimens that were consolidated over shorter times. Also, the liquefaction strengths were observed to be relatively large in samples containing a larger amount of fine fraction material.

The second part of the study examines the strength of the ground motion of the three earthquakes described in ii). In addition, soil data from liquefied areas during the past two earthquakes, changes in the liquefaction strength by the “aging” effect obtained from the test results in the first part of the study, and the magnitude of the earthquakes were used to determine why the area around the old Sumida River was not subjected to liquefaction. Based on the results, the area was not liquefied by the Great East Japan Earthquake in spite of the occurrence of liquefaction during the past two earthquakes because of the increases in the liquefaction strength due to the “aging” effect, as well as the presence of relatively small ground motions that occurred during the most recent earthquake event.

Keywords: Great East Japan Earthquake, Wooden house, ”Aging” effect.

1. Introduction

On March 11, 2011, the Great East Japan Earthquake caused extensive soil liquefaction over a wide expanse of land in Japan, extensively damaging wooden houses, water supplies, and sewer systems. Liquefaction also damaged the bay coast of landfills in Tokyo, but did not reach the alluvial lowland area in the immediate vicinity of Tokyo Bay. This vicinity includes the old Sumida River, located between the Adachi and Katsushika wards of Tokyo (see Fig. 1), in which (according to historical records) liquefaction occurred during the Great Kanto Earthquake of 1923 and the Edo Earthquake of 1855. The reason this area escaped liquefaction during the Great East Japan Earthquake but not in previous earthquakes can be understood from two perspectives:

i) Liquefaction strength increases over time by the so-called "aging" effect. The liquefaction strength increases by long-term constraint or subjection of the soil to a shear history. Eventually, the soil becomes resistant to liquefaction. Tatsuoka et al. (1988) conducted cyclic triaxial tests on soil samples, and concluded that liquefaction strength is increased by a long-term consolidation state. The aging effect is potentially significant because 90 years separate the Great Kanto Earthquake from the Great East Japan Earthquake.

ii) The ground motion of the Great East Japan Earthquake was weaker than in the previous two earthquakes. Although the Great East Japan Earthquake occurred on a larger scale than the Great Kanto and Edo earthquakes, Tokyo was sufficiently far from the epicenter. In contrast, the epicenters of the Great Kanto Earthquake and the 1855 Edo Earthquake were close to Tokyo, inducing a large shock in that area.

In light of the above, we examined the factors responsible for liquefaction during the three earthquakes in this area by sandy soil tests and a simplified liquefaction judgment scheme.

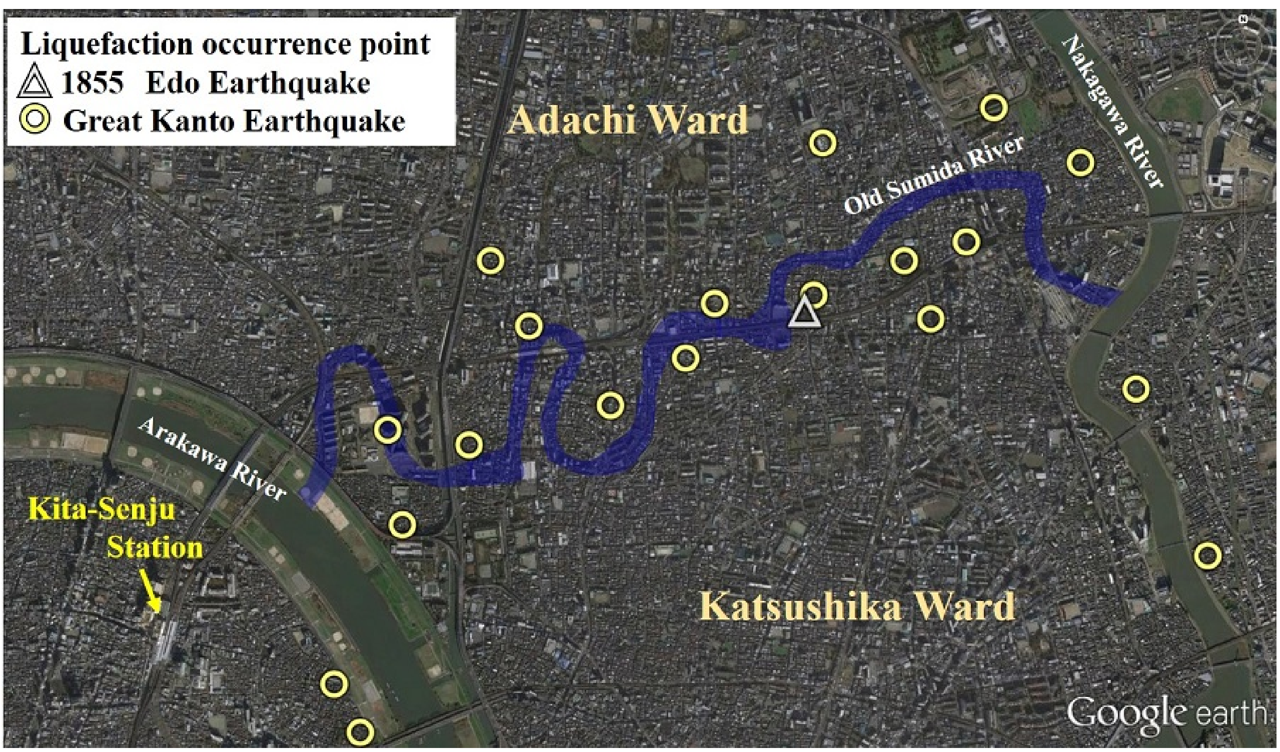

Fig. 1 – Liquefaction history around the old Sumida River

2. Study of aging effect due to cyclic triaxial test

2.1 Test Description

The Great East Japan Earthquake caused liquefaction damage and sand boiling even in Urayasu, Chiba Prefecture. The sand boil (hereafter termed Urayasu sand) was harvested for the liquefaction test. The Urayasu sand, which contains many fine fraction, was divided into coarse and fine soils by sifting through a 75-μm sieve in water. The weight ratio of the fine soil was adjusted to 0, 30 and 60% of mixed coarse soil. Table 1 shows the physical test results, and Fig. 2 shows the grain size distribution curves of the Urayasu sand after particle size adjustment. The grain size distribution curve of the sand boil picked up in Urayasu is also shown in Fig. 2.

The relative densities were determined by the conventional maximum and minimum density test method (JIS A 1224). However, this method can be applied only to the sandy soil of the fine fraction content of less than 5%, i.e., the method of JIS A 1224 cannot be applied to Urayasu sand. Therefore, the maximum dry density was determined by alternative methods; namely, by increasing the number of blows (Test Method A), adding an overburden pressure 0.206 kPa to the test method A (Test Method B), and a compaction test (JIS A 1210). The conditions of each test case are shown in Table 2.

Figure 3 shows the maximum dry density obtained in each test method. Test method B yielded the largest maximum dry density for all samples, without destroying the soil particles. Thus, in subsequent analyses, the maximum dry density (used to define the relative density) was obtained by test method B.

The liquefaction test was performed in a cyclic undrained triaxial test apparatus. Each specimen was 10 cm high and 5 cm in diameter. Given the large fine fraction of Urayasu sand, we discarded the air-pluviation as a specimen fabrication method, because the particle size composition could be changed by tossing the particles in the air. Instead, a funnel was inserted in the mold, and the sample was divided into five layers. To ensure uniform density throughout the specimen, the sides of the mold were tapped by a vibrating mallet. However, the D_r80% specimen was difficult to prepare by the dry vibrating method, so was fabricated by the dry compacting method. The effective confining pressure was 50kPa, and the consolidation time for the effective confining pressure in a container of cyclic undrained triaxial test apparatus was 1 hour.

To examine the influence of long-term consolidation, the consolidation period was set to 10, 30, and 100 days. The consolidation test was performed on loose (D_r50%) and dense (D_r80%) samples. Figure 4 is a schematic of the compaction device prepared for the long-term consolidation. The specimens were prepared in a predetermined mold as described above, and a dead load of 50kPa was applied to the top surface of the specimen immersed in water.

Figure 5 shows the flow of cyclic undrained triaxial test of each consolidation method.

Table 1 – Summary of laboratory test results

Sample	**Fc(%)**	**ρ_s(g/cm^3)**	**ρ_{dmax}(g/cm^3)**	**ρ_{dmin}(g/cm^3)**	**I_p**
A	9.0	2.621	1.418	1.059	NP
B	39.2	2.633	1.572	1.109	0.8
C	64.2	2.685	1.598	1.072	0.4

Table 2 – Methods to test the maximum density

Method	**JIS A 1224**	**Method A**	**Method B**	**JIS A 1210**
The number of blows	1000	6000	6000	A-a method
Weight (Overburden pressure)	–	–	600 g (0.206 kPa)	

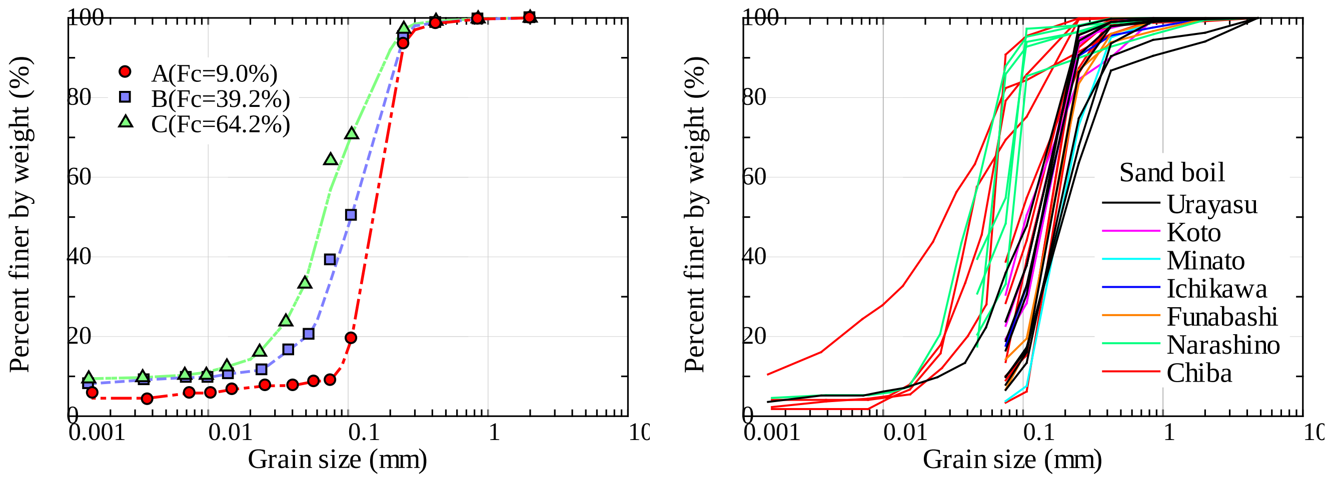

Fig. 2 – Grain size distribution curves of sands with different fine fractions

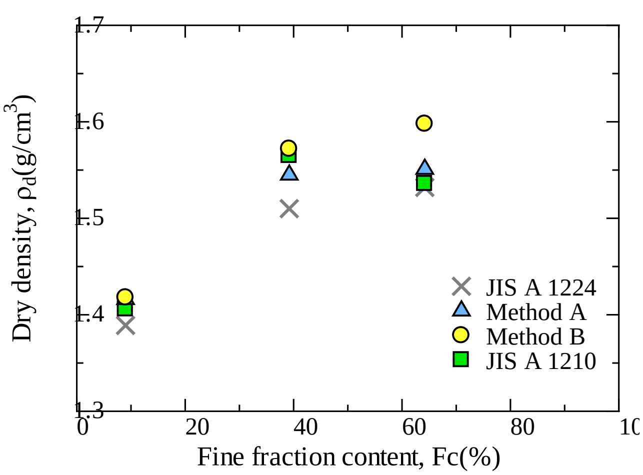

Fig. 3 – Results of maximum dry density test

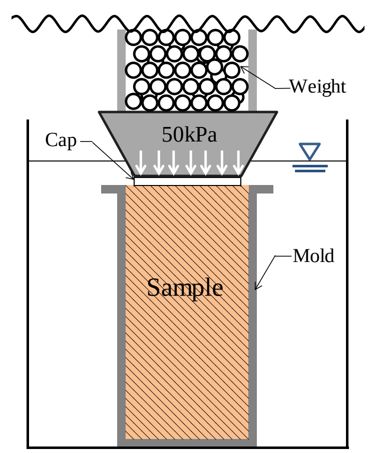

Fig. 4 – Schematic of long- term consolidation setup

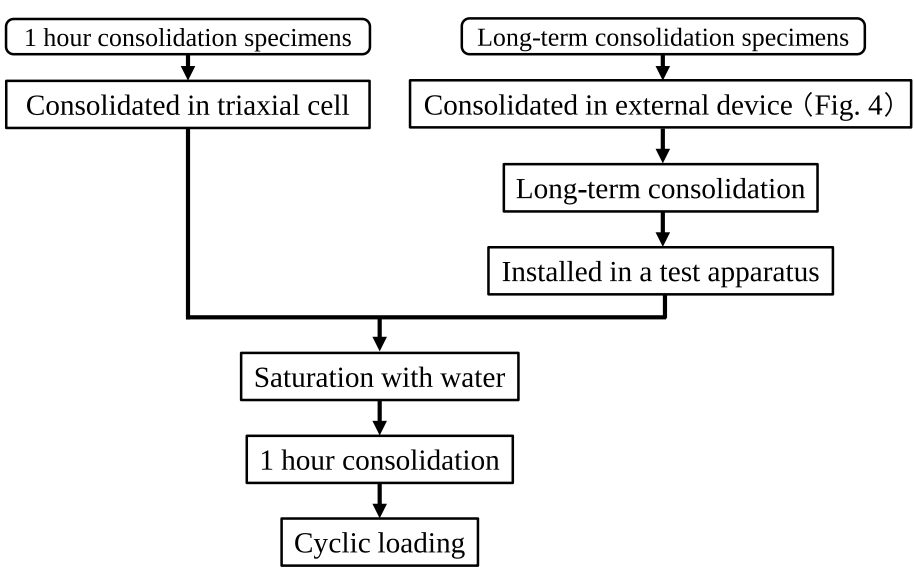

Fig. 5 – Flow diagram of the cyclic undrained triaxial test

2.2 Test Results

Figure 6 shows an example of the liquefaction test results. When double amplitude axial strain "ε_{DA}" than the test results reached 5%, specimens were judged to be liquefied. From these results, a relationship produce between the cycle number and cycle stress amplitude ratio when the ε_{DA} reaches 5% as shown in Fig. 7, the liquefaction strength ratio "R_{L20}" was defined as the cycle stress amplitude ratio when the cycle number is 20 times.

Figure 8 shows the change in liquefaction strength ratio of each sample as functions of relative density from 50 to 80%. For all samples, increasing the density increased the liquefaction strength, but the extent of the change depended on the fine fraction contents. From these results, we can determine the liquefaction strength ratio at a certain density of Urayasu sand.

Long-term consolidation increased the liquefaction strength ratio at all densities and fine fraction content. The liquefaction strength was especially improved in loose samples containing many fine grains. Figure 9 shows the relative density changes in the samples at various times during the long-term consolidation. The loose samples exhibit the largest density changes throughout the consolidation, suggesting that densification is largely responsible for increasing the liquefaction strength.

Figure 10 plots the liquefaction strengths of the compacted specimens as functions of time during the long-term consolidation with the relationships proposed previously by Yasuda et al. (2003). The rate R_{tc} of the liquefaction strength ratio in Fig. 10 was calculated as follows:

$$R_{tc} = \frac{R_{L20}\text{ of each specimens long} - \text{term consolidation}}{R_{L20}\text{ of each specimens 1 hour consolidation (Fig. 8)}} \tag{1}$$

The rise in liquefaction strength over long-term consolidation differs among the samples and conditions. The R_{tc} was maximized at 1.4 times after 100 days. However, the R_{L20} of the 100-day consolidation specimens was significantly lower in Sample A than in the other samples. As shown in Fig. 10, this specimen is slightly less dense than the specimens prepared under other conditions. However, as the density does not significantly change among the samples in Fig. 9, the cause of the low R_{L20} in Sample A is unknown at this time.

Figure 11 plots the stress-pass and stress–strain curves of Sample A after 1 hour consolidation and long-term compaction. In these tests, the same stress cycle was repeated until the specimen consolidated for 1 h became liquefied. After long-term consolidation, the stress–strain response was much more gradual, indicating high resistance to liquefaction. The same tendency was observed in the dense samples (Fig. 12).

These results confirm that liquefaction strength increases after long-term compaction. Other than density effects, the liquefaction is proposed to increase by the following mechanisms:

i) The soil particles become bound by chemical adhesive forces during long-term consolidation.

ii) Unstable particles gradually settle to a state of optimal stability.

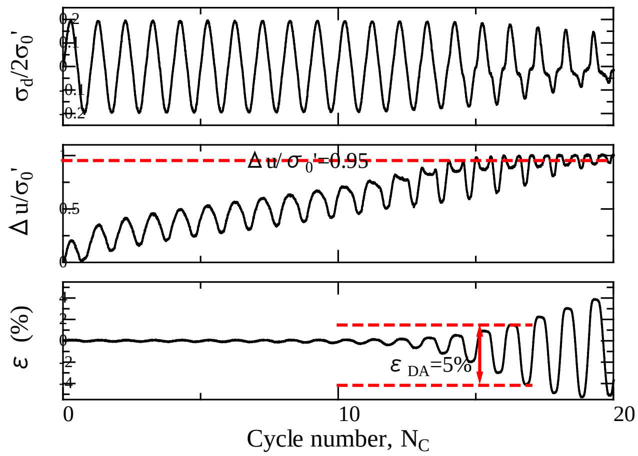

Fig. 6 – Examples of cyclic undrained triaxial test results

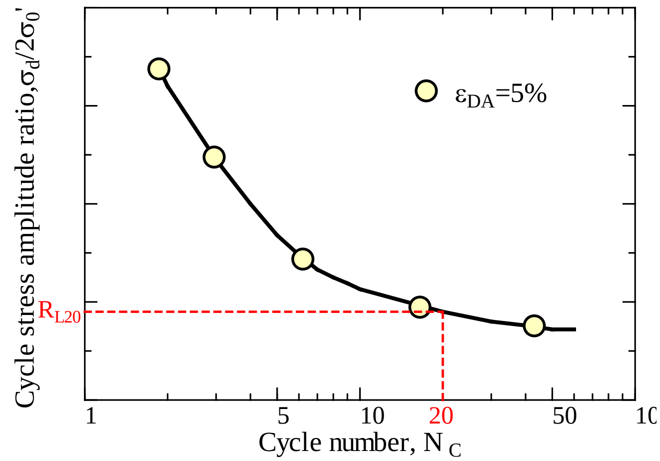

Fig. 7 – Definition of liquefaction strength

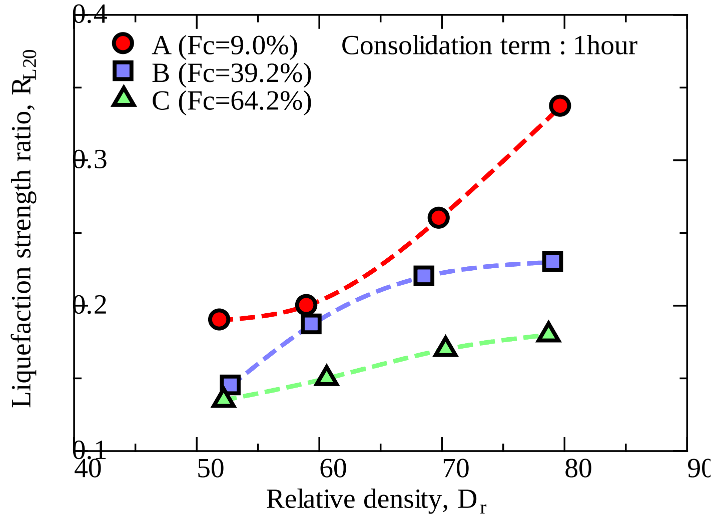

Fig. 8 – Relationship between the relative density and liquefaction strength ratio

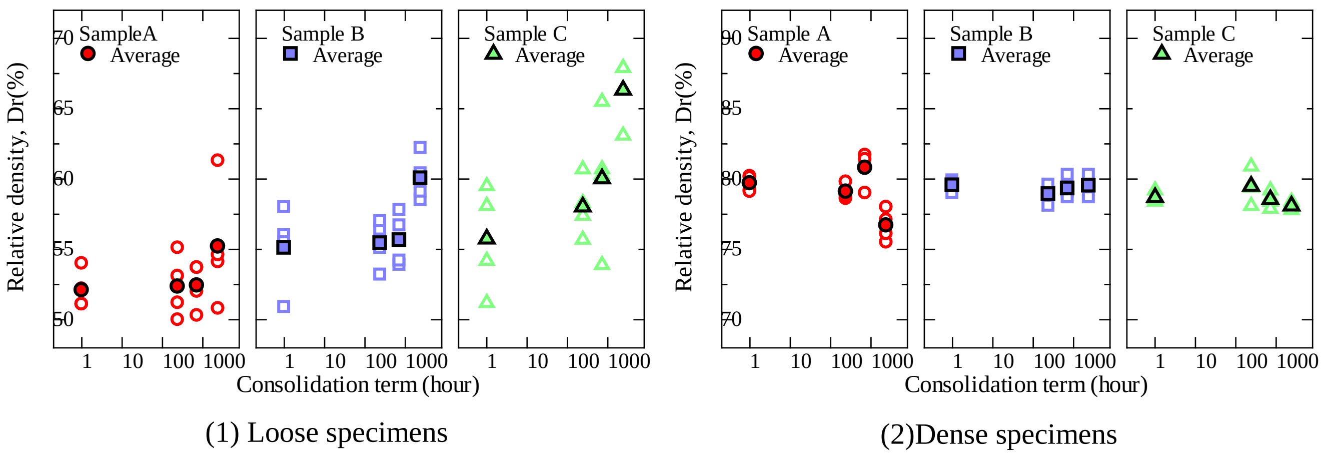

Fig. 9 – Density changes during long-term compaction

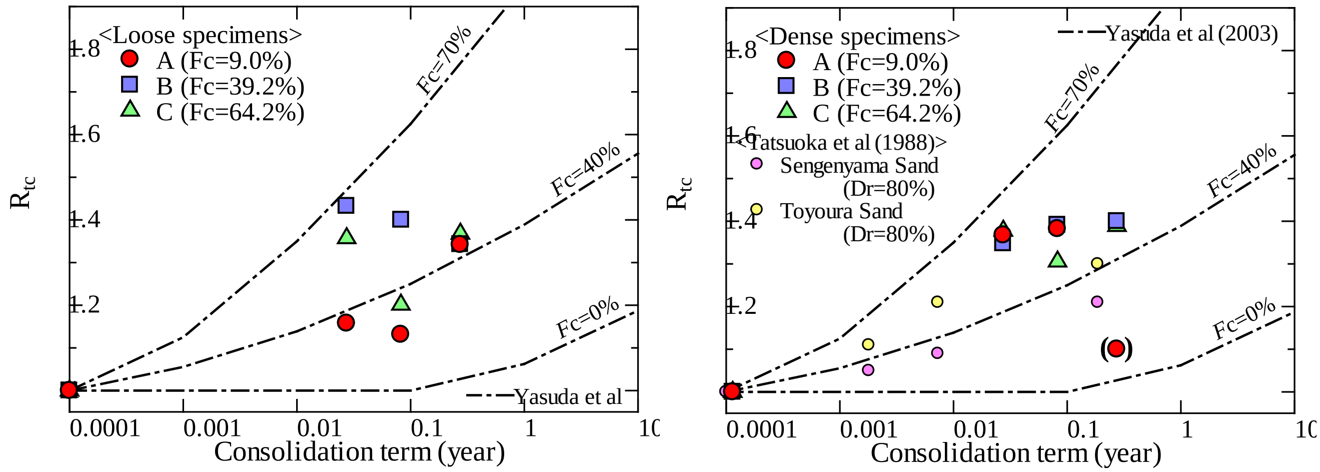

Fig. 10 – Liquefaction strength growth rate throughout the consolidation term

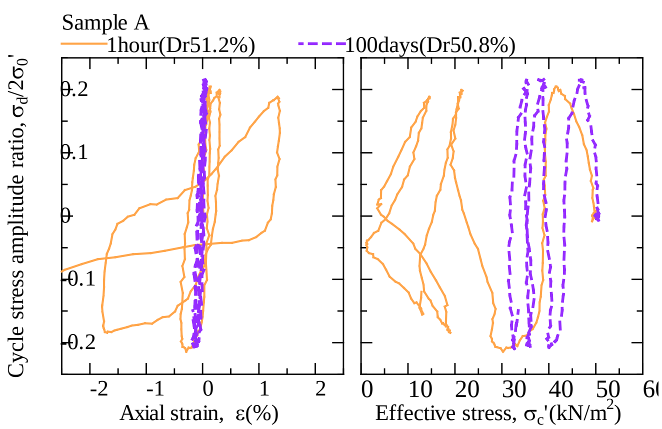

Fig. 11 – Effects of sustained consolidation on stress pass and stress-strain relation in loose specimen

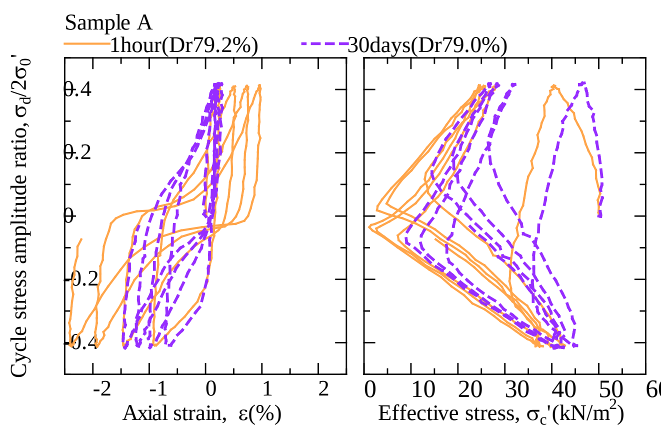

Fig. 12 – Effects of sustained consolidation on stress pass and stress–strain relations in dense specimen

3. Study on liquefaction history of old Sumida River area

3.1 Condition Setting

Figure 13 shows the geomorphological classification of the old Sumida River area, which was the flow path of the Tone River. This area is mainly formed from natural levee, the back marsh, and the old river channel. As shown in Fig. 1, the liquefaction points of past earthquakes are concentrated around the old river channel. Therefore, the present study focused on the old river channel and the natural levee. The boring data in the Adachi district in Tokyo were collected at the sites indicated in Fig. 13. These 48 data have been measured between 1963 and 2012.

Table 3 states the peak ground acceleration of each earthquake. For the Great East Japan Earthquake, the maximum surface acceleration of the ground was recorded by the strong motion observation network K-net. The ground motions of the Great Kanto Earthquake and the 1855 Edo Earthquake were not measured, as ground-motion observation systems were not installed. Therefore, their surface accelerations were estimated from the seismic intensity distributions obtained from the extent of damage to houses and buildings the sites.

The liquefaction induced by each earthquake was evaluated by the Liquefaction potential Index Number (P_L value):

$$P_L = \int_0^{20} (1 - F_L)(10 - 0.5x)dx \tag{2}$$

where x is the depth from the ground surface (m) and F_L denotes the safety factor against liquefaction (F_L value). At each depth, the F_L is calculated as:

$$F_L = \frac{R}{L} \quad \begin{cases} F_L \leq 1.0\text{: judged as liquefied} \\ F_L > 1.0\text{: judged as not liquefied} \end{cases} \tag{3}$$

where R is the in-situ cyclic strength ratio, and L is the seismic shearing stress ratio. R can be calculated from the soil cyclic triaxial strength ratio (R_L) by the compensated equation:

$$R = C_w R_L \tag{4}$$

where the calibration coefficient C_w depends on the seismic motion and the anisotropic consolidation. The Great Kanto Earthquake and the 1855 Edo Earthquake determines the correction coefficient according to the based on the specifications for highway bridges, JRA (2002). So the Great Kanto Earthquake is treated as TYPE1 ground motions because it is plate boundary earthquake. On the other hand, as the type of the 1855 Edo Earthquake was not clear, both C_w were adopted.

$$C_w = 1 \qquad \text{(TYPE1)} \tag{5}$$

$$C_w = \begin{cases} 1.0 & (R_L \leq 0.1) \\ 3.3R_L + 0.67 & (0.1 < R_L \leq 0.4) \\ 2.0 & (0.4 < R_L) \end{cases} \qquad \text{(TYPE2)} \tag{6}$$

For the ground motion of the Great East Japan Earthquake, we adopted the correction coefficient proposed by Ishikawa et al. (2014):

$$C_w = 0.46 \times {R_L}^{-0.43} \qquad \text{(Ishikawa et al (2014))} \tag{7}$$

For other calculations was calculated based on specifications for highway bridges (JRA(2002)).

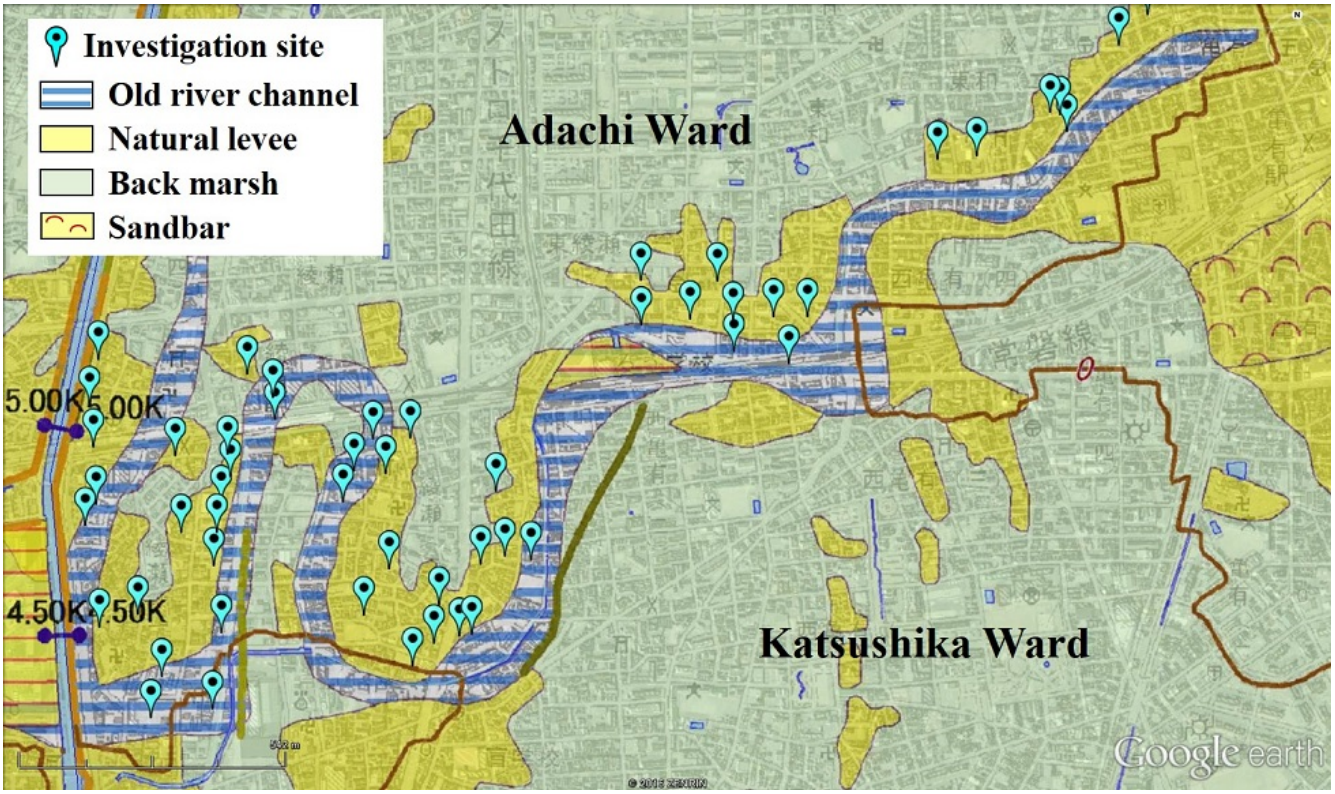

Fig. 13 – Geomorphological condition and investigation spot around old Sumida River

Table 3 – Peak ground acceleration of each earthquake

	1855 Edo Earthquake	**1923 Great Kanto Earthquake**	**2011 Great East Japan Earthquake**
PGA(cm/s^2)	450	350	200
Kind of ground motion	Unclear (Probably near-field)	Plate boundary	Plate boundary
Age difference from the boring data (±25)	-132 year	-64 year	+23 year

3.2 Liquefaction judgment result

Figure 14 presents the liquefaction judgment results of each earthquake. Based on the P_{L} value, the liquefaction extent was assigned to one of four categories of increasing severity:

$$\begin{array}{ll} P_L = 0 & \text{There is no possibility of damage caused by liquefaction} \\ 0 < P_L \leq 5 & \text{There is a low possibility of damage caused by liquefaction} \\ 5 \leq P_L < 15 & \text{There is a high possibility of damage caused by liquefaction} \\ P_L \geq 15 & \text{There is a very high possibility of damage caused by liquefaction} \end{array} \tag{6}$$

This judgment revealed that natural levee sites were more vulnerable to liquefaction than the old river. This result verifies the integrity of the past liquefaction history. The sites reported as liquefied on a large scale in the Great Kanto Earthquake was frequently classified as high possibility of liquefaction in the corresponding judgements.The sites reported as liquefied in the 1855 Edo Earthquake and Great Kanto Earthquake were frequently classified as high possibility of liquefaction in the corresponding judgements. In contrast, most of these sites were at low risk of liquefaction in the judgment of the Great East Japan Earthquake.

As mentioned before, the ground motion type of the 1855 Edo Earthquake was not clear. In Fig. 14, C_{w} is assumed as 1.0 based on Eq. (5). However, the 1855 Edo earthquake had the large estimated seismic intensity, and it may be better to judge the Edo earthquake was to be the near-field earthquake and added the judgment due to the near-field earthquake also Eq. (6). The judgment result is shown in Fig 15. In the near-field earthquake, liquefaction potential index of the 1855 Edo earthquake became the same grade as the 2011 Great East Japan Earthquake.

However, the aging effect is not taken into consideration by in this figure. The year when the soil investigations shown in Fig. 13 was about 130 years and 64 years after the Edo earthquake and the Kanto earthquake, respectively. And about 23 before the Great East Japan earthquake.

By considering the aging effect shown in Fig. 10, the actual PL values must be larger than the calculated ones shown in Figure 15 for the Edo and the Kanto earthquakes, and vice versa for the Great East Japan Earthquake. So, by considering the aging effect. it can be explained that liquefaction occurred during the Edo earthquake and did not occurred during the Great East earthquake though PL values for two earthquakes are almost same as shown in Fig.15.

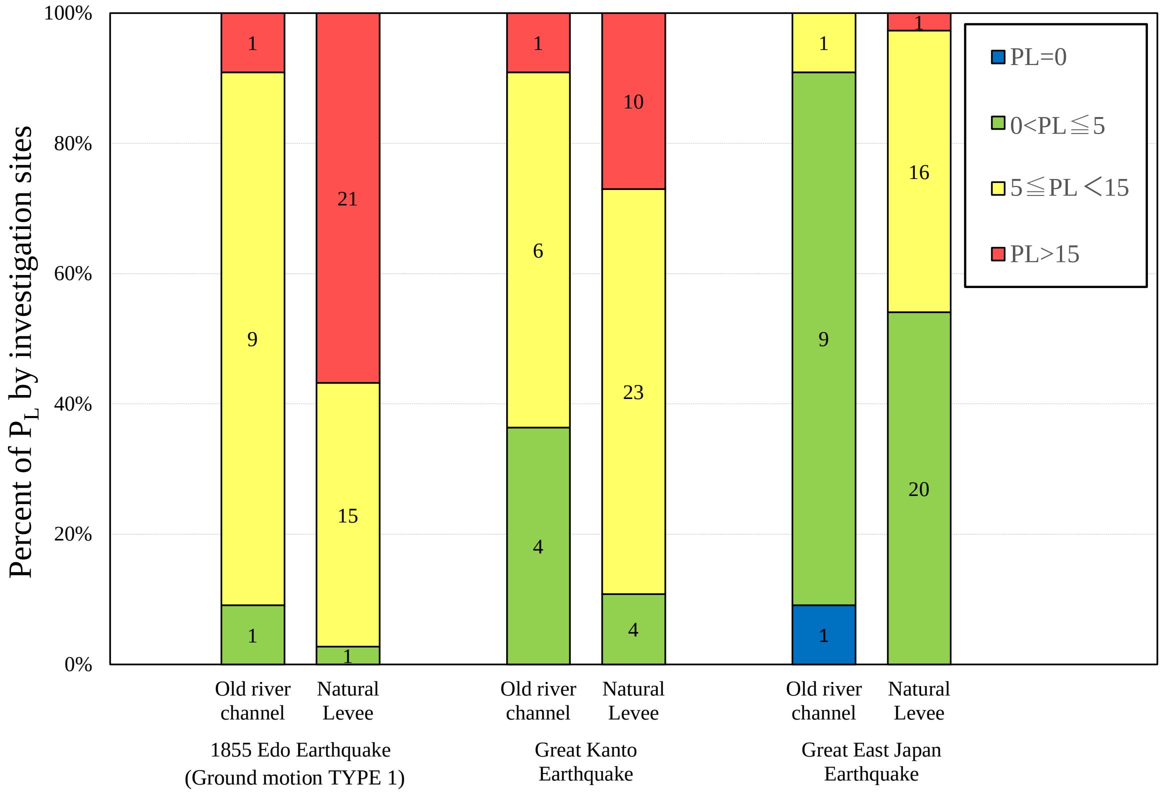

Fig. 14 – Liquefaction judgment results of the three earthquakes around old Sumida River

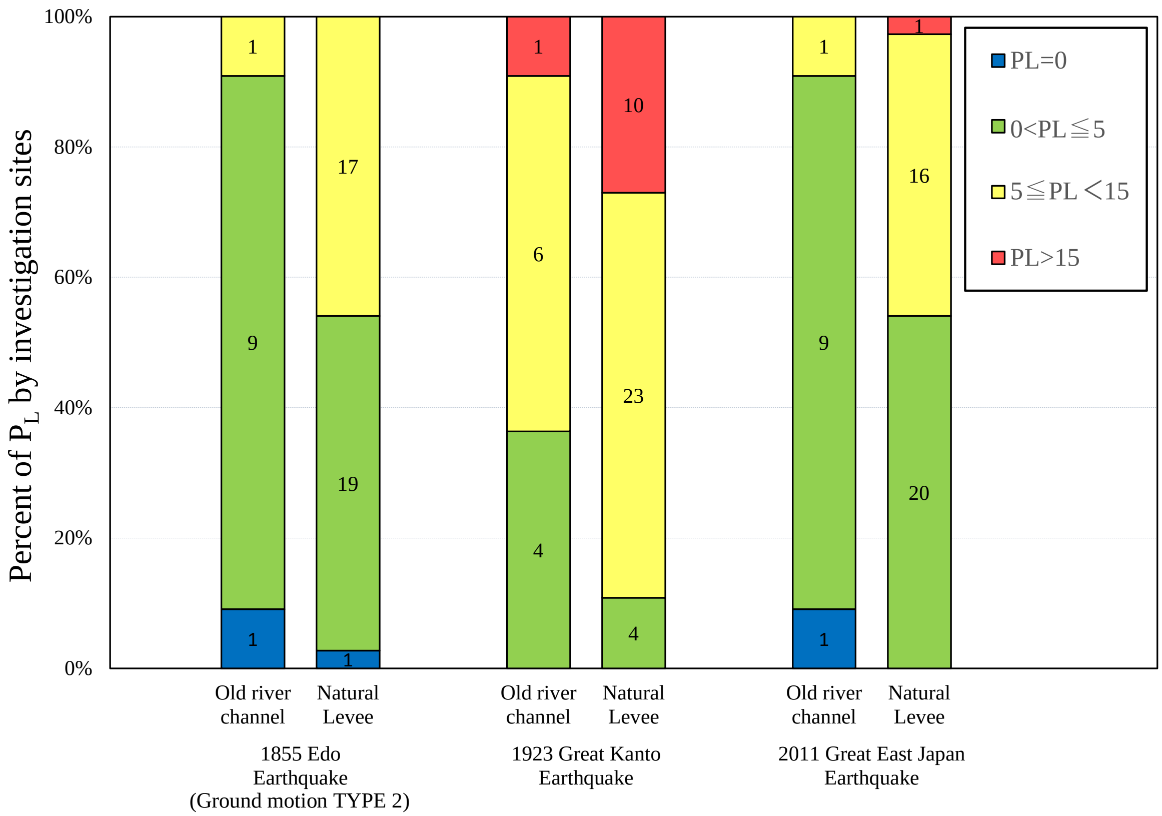

Fig. 15 – Liquefaction judgment results of the three earthquakes around old Sumida River

4. Conclusions

To investigate the earthquake-related liquefaction history of lowlands in the Tokyo area, we performed liquefaction tests of sand specimens subjected to long-term consolidation and investigated the liquefaction history of the old Sumida locality. The following conclusions were derived from the study:

1) Long-term consolidation (up to 100 days) significantly increased the liquefaction strength of Urayasu sand. The strength improvement was approximately 1.4 times at all densities and fine fraction contents. In the loose samples, increased liquefaction strength is expected by the increased density throughout long-term consolidation.

2) From the liquefaction judgment results of the old Sumida River, the liquefaction conditions were largely governed by ground motions during the past three earthquakes. However, the possibility of liquefaction in the natural levee was lower during the Great East Japan Earthquake than in the earlier earthquakes, suggesting that aging also plays a role.

5. References

[1] Wakamatsu K (2011): Liquefaction history map of Japan in 745-2008. (in Japanese).

[2] Tatsuoka F, Kato H, Kimura M, Tej B.S. Pradhan (1988): Liquefaction strength of sands subjected to sustained pressure. *Soils and Foundations*, Vol.28 No1, 119-131.

[3] Yasuda S, Shimizu Y, Koganemaru K, Morimoto I (2003): Aging effect of sandy soils on liquefaction strength, Deformation Characteristics of Geomaterials, IS Lyon03, Balkema, 1319-1324.

[4] Geospatial Information Authority of Japan “Flood control terrain classification map” Japan (http://maps.gsi.go.jp/).

[5] Adachi ward of Tokyo “Map information providing service” Japan (http://www.sonicweb-asp.jp/adachi/)

[6] National Research Institute for Earth Science and Disaster Prevention (NIED) “K-NET WWW service.” Japan (http://www.kyoshin.bosai.go.jp/kyoshin/).

[7] Morimoto K (1980): Ground motion of the 1923 Great Kanto Earthquake. *Architectural Institute of Japan paper report collection*, No289, 79-91.

[8] Huanan T, Yamazaki F (1996): Relationship between Ground Motion Indices and New JMA seismic Intensity. *Production Research Bulletin*, Vol.48 No. 11, 31-34.

[9] Ishikawa K, Yasuda S, Aoyagi T (2014): Studies on the reasonable liquefaction-prediction method of the 2011 Great East Japan Earthquake. *Journal of the Japanese Geotechnical Society*, 9(2), 169-183.

[10] Japan Road Association (2002). Specification for highway bridges. (in Japanese).